SOCIETY FOR SCIENCE AND EDUCATION UNITED KINGDOM

JBEMi JOURNAL OF BIOMEDICAL ENGINEERING AND MEDICAL IMAGING

ISSN: 2055-1266
VOLUME 2 ISSUE 4

Application of Ex Vivo Cryo-imaging Technique for Three-Dimensional Finite Element Analysis of Atherosclerotic Plaque Rupture

Ahmad Abdul-Aziz[1], Ross Cotton[2], Simon Richards[2], Ali Faramarzalian[3], Philippe G. Young[2], Daniel Chamie[5], David L. Wilson[4], Hiram G. Bezerra[5], Marco A. Costa[5]

[1]University of Michigan, Dept. of Internal Medicine, Ann Arbor, MI 48109, USA
[2]Simpleware Ltd, Exeter, United Kingdom
[3]School of Medicine, Case Western Reserve University, Cleveland, OH 44106, USA
[4]Department of Radiology, Case Western Reserve University and University Hospitals Case Medical Center, Cleveland, OH 44106, USA
[5]Division of Cardiology, Harrington-McLaughlin Heart and Vascular Institute, University Hospitals Case Medical Center, Case Western Reserve School of Medicine, Cleveland, OH 44106, USA
ali920@yahoo.com

ABSTRACT

Cryo-imaging is an ex vivo vascular imaging modality that acquires serial 2D fluorescence and bright-field images at 20µm increments without sacrifice to tissue morphology. These features make Cryo-imaging an attractive approach for rendering high-resolution 3D volumes that may serve as a basis for finite element analysis (FEA) studies of plaque rupture. This work demonstrates the first use of Cryo-imaging for the imaging of a human coronary vessel and the subsequent ren-dering of a 3D FE model that clearly delineates critical anatomical features of atherosclerotic plaque. FEA is then performed to assess the plaque rupture conditions that result in a thrombotic episode.

Keywords: Cryo Imaging, Finite Element, Plaque Rupture, Ex Vivo, atherosclerotic lesion

1 Introduction

In Western countries, acute coronary syndromes (ACS) are the leading causes for hospitaliza-tion [1]. A major cause of ACS is plaque rupture which has been detected in 60 to 70 percent of cases [2]. Vulnerable plaques which are also referred to as thin cap fibroatheromas (TCFA) possess several histological characteristics—a thin fibrous cap (<65µm), a lipid pool, and in-flammation near the fibrous cap [3, 4, 5]. A silent atherosclerotic lesion ruptures when acti-vated macrophages, T cells, and mast cells produce molecules such as inflammatory cytokines, proteases, coagulation factors, radicals, and vasoactive molecules that weaken the fibrous cap [5]. Once the fibrous cap has been weakened, it is then subject to mechanical stressors which induce its rupture.

Investigation of the biomechanics of atherosclerosis has relied upon finite element analysis (FEA) for computing stress and strain distributions in hypothesized vascular cross-sections or more realis-tic morphology derived from histology of autopsy specimens [6]. FEA is a technique that allows re-searchers to go beyond simple image analysis. It allows for the rendering of accurate finite element models that

DOI: 10.14738/jbemi.24.1335
Publication Date: 22nd July 2015
URL: http://dx.doi.org/10.14738/jbemi. 24.1335

represent the true geometry of the object being analyzed and enables the evaluation of the stress and strain distribution regardless of its geometric complexity [7].

Histology currently serves as the gold standard for the determination of plaque composition and geometry [8-11]. Histology offers excellent resolution and through the application of tissue-specific stains, can provide clear delineation of tissue composition [8-11]. However, there are also several drawbacks associated with histology. During histology processing, the tissue shrinks and reforms from its natural shape. In addition, the manipulation of samples as thin as 5-10 µm may results in further warping, folding, and tearing of the tissue [7, 12]. As a result of the artifacts that may occur during histological processing, the accuracy of geometric models for biomechanical analysis is lim-ited.

Although histology-based FEA studies have offered valuable insight into the various mechanical stressors that induce plaque rupture, they have been limited to 2D analysis. Furthermore, con-structing 3D histology-based FEA models would not only require a large number of samples, but it would also be extremely expensive and time consuming. Moreover, accurately registering image slices taken by conventional histology to in-vivo vascular imaging modalities is also error prone.

A need for a more accurate approach to modeling the mechanical behavior of vulnerable plaques is critical to defining the conditions that induce plaque rupture. Therefore, a construction of 3D FEA models based on Cryo-imaging [12] is essential to carry out a meaningful analysis. In 2006, Cryo-imaging was introduced as a tool for the validation of intravascular imaging modalities. Cryo-imaging utilizes a large-specimen cryo-microtome with a mounted episcopic microscope and charge-coupled device (CCD) camera to obtain block face images of embedded frozen tissue samples [12]. Cryo-imaging acquires serial 2D fluorescence and bright-field images at 20 µm increments without sacrifice to tissue morphology. These features make cryo-imaging an attractive means for rendering high-resolution 3D volumes that serve as a basis for FEA studies of plaque rupture.

In this current study, we demonstrate the first use of Cryo for the imaging of a human coronary vessel and the subsequent rendering of a 3D finite element model that clearly delineates critical anatomical features of ather-osclerotic plaque. FEA is then performed in order to assess the plaque rupture conditions that result in a thrombotic episode.

2 Methods

2.1 Specimens

One left anterior descending artery (LAD) was obtained from human cadavers from the Cuyahoga County Cor-oner's office. After removal from the bodies, vessels were stored at 4 °C until Cryo-imaging was performed. Approval was obtained from the Case Institutional Review Board to work with all specimens in compliance with federal, state, and local laws.

2.2 Cryo-imaging

The frozen vessel was removed from the rig and cut with a band saw resulting in several 30 mm cylindrical blocks. Blocks were placed in the cryo-imaging system to equilibrate to a -20° C cutting temperature. They were then mounted onto the cryo-microtome stage (8250 Large Section Cryostat, Vibratome, St.Louis, MO, U.S.A.). For each segment, 50 µm sections were cut (distal to proximal) until a point had been reached

where the vessel was clearly smooth and visible with no artifacts. A digital CCD camera (Retiga Exi, QImaging, Surrey, BC, Canada) attached to a stereo microscope (SZX12, Olympus, Tokyo, Japan) was used to capture images of the block face. A bright light illuminator was used for bright field images. Blue light excitation (460-490 nm) and green fluores-cent protein (GFP) emission (510nm) filters were used for to capture fluorescence images. Exposure times were 10 ms, (milliseconds), for bright-field imaging and 3000 ms for fluorescence imaging. Both images were obtained using the same RGB wheel (RGB-Slider, Q Imaging).

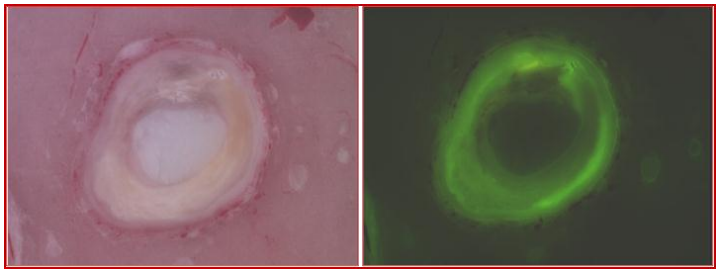

Figure 1. 2D cross-sectional slice of vessel taken by Cryo. Bright field (L) and fluorescent (R).

White balance and exposure times were calibrated using a white sheet of paper and manufacturer software auto-calibration functions, respectively. Bright-field images were divided by the white image to correct for the uneven illumination. Per block face, one bright-field image then one fluorescence image was captured at the same magnification. A 20 µm slice was cut, and another set of images was taken of the new block face. This process was repeated across the length of the vessel in order to obtain a longitudinal volume of consecutive images.

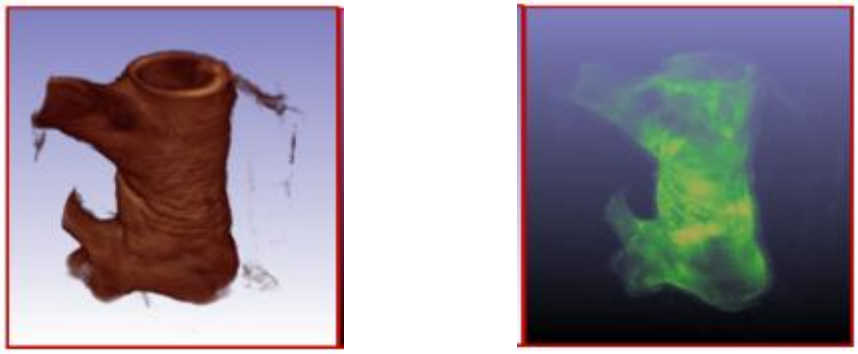

a)3D Volume model of the artery vessel b) Transparent view of the vessel model

Figure 2. 3D Volume rendering of re-assembled Cryo sectioned stack of images

2.3 Visualization

The 2D fluorescent images were then imported into the software ScanIP [13], where a 3D volume rendering of the complete image stack can be generated (Figure 2). Adjusting the mapping of this volume rendering option allows unique high quality images to be generated prior to performing segmentation. Note that in Figure 2 two different views are reported showing the results obtained from the volume rendering process where a transparent and 3D volume model of the arteries was generated. Additionally, as stated earlier, Cryo-imaging acquires serial 2D fluorescence and bright-field images at 20 µm increments without

sac-rifice to tissue morphology which allow more precision and highly accurate 3D volume representation of the model.

2.4 Image Processing

The images then underwent segmentation to delineate the tissue components that are present in ather-osclerosis. The following components were included in this study and have been previously validat-ed—vessel wall, lipid, calcium, and plaque [12]. The fluorescent fibrosis was segmented with ScanIP [13] using basic threshold segmentation, allowing the high intensity pixels of the fluorescent fibrosis to be de-lineated. The remaining regions (vessel wall, lipid and fibrous cap) required a combination of thresholding, floodfill, morphological filters, and Boolean operations between parts to segment the regions. It is im-portant to note that these operations are applied over the entirety of the 2D image stack.

It should be noted that the image processing technique is applied in this study is fairly reproducible, a script can be generated with the software and customized to carry out the image processing with great simplicity. The process applied in creating the finite element mesh based on the image segmentation is very intense and quite complicated. Further, due to the proprietary nature, only a limited description is permitted about the algorithms used in the software to carry out the image processing and segmentation. Therefore, reproduction of other segments of the vessel samples are achievable and the technique is fairly straight forward once an initial sample is demonstrated. However, it should be noted that the potential for propagated error in the analysis is very minimal since each sample is a treated as new entity or a new model and segmentation adjustment is made accordingly to ensure that accuracy is preserved.

3 3-D Segmentation Rendering and Finite Element Mesh Generation

The image segmentation process was followed with the visualization of the 3D volume, Figure 3, and then with finite element mesh generation. The aim was to take the verified segmentation of the artery test sample and generate a finite element multi-part mesh of the vessel indicating the layers of lipid and other materials.

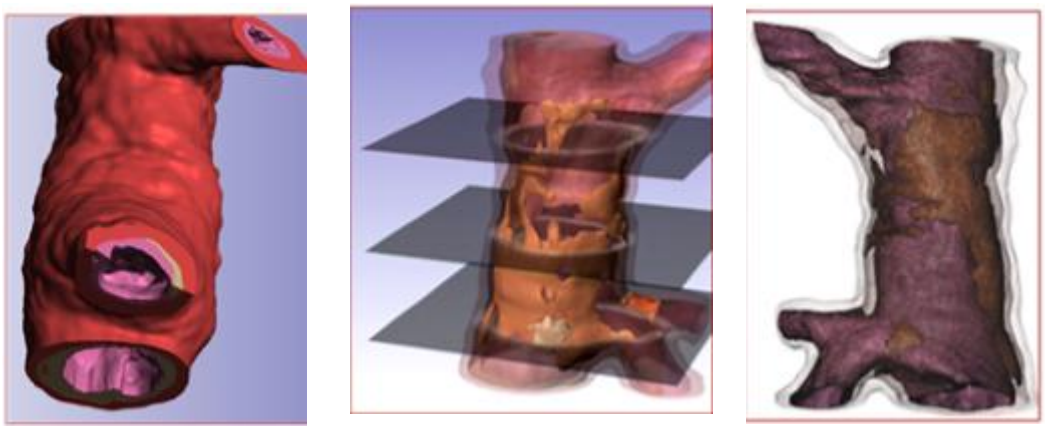

a)3D volume vessel model b) Sectioned views c) 3D Mesh

Figure 3. Segmented 3D volume view of the coronary vessel.

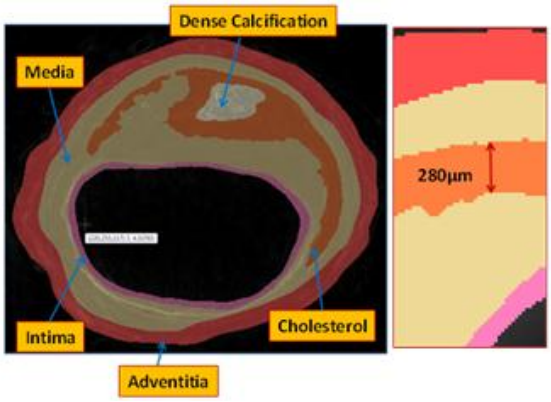

Figure 4. A typical cross-sectional slice through the vessel taken by Cryo-Imaging and segmented.

A cross section showing lipid, calcification, cholesterol, and components of the vessel wall can be seen in Figure 4. ScanIP+FE [13] is used to generate a number of finite element meshes based on the 3D segmented image data [13]. The automated mesh generation of the multiple regions pre-serves interface conformity with shared nodes. The final finite element mesh consisted of 1,044,037 four nodes tetrahedral elements and 204,168 nodes, Figure 5.

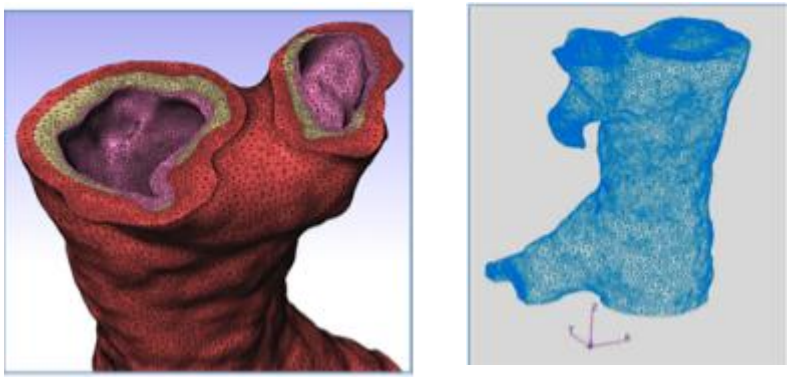

(a) Visualization model b) Finite element mesh

Figure 5. Visualization of the coronary vessel with various materials details and finite element mesh.

The density of meshes generated in ScanIP+FE is closely connected to image resolution in order to explore the convergence of results (field parameters of interest); the image was down sampled to create two volumes of the vessel geometry in order to generate, respectively, high and low resolution models. An interesting point can be made here about image based models versus CAD models. In CAD models, the geometry of the model is assumed to be exact and mesh density is increased principally in order to obtain a better model of the field parameters of interest (say the stress field within a loaded structure). In contrast, both the response and the geometry of the system are approximated in image based models which is the case in this study.

By generating models based on increasing image resolutions, one not only improves the modeling of the re-sponse, but also the representation of the geometry (one effectively converges to the geometry). Hence, one can perform essentially a dual or coupled convergence study which will provide powerful arguments for the validity of the simulations as convergence of results demonstrates not only that the

mesh is of sufficient density to capture the field parameter of interest but also, and as importantly, that the image resolution on which the model is based is high enough to capture relevant features in the scanned object.

4 Finite Element Analysis

FEA was carried out using Abaqus finite element code [14]. The numerical analyses were made under linear elastic conditions where the behavior of the material is defined by the two material constants—Young's modu-lus and Poisson's ratio. Materials constants were obtained from Table1 [8-11, 15-17]. Isotropic linear condi-tions were assumed where the modulus (E) and the poison's (P) ratio were assumed to be equal in all directions. R direction represents the properties in the radial direction, θ is the tangential direction and Z is along the length of the artery. Directions rθ, θz and zr are the in visual plane defined by each direction respectively. It was assumed that the lipids and calcifications were nearly incompressible because of the high water content in the case of lipids and high comparative stiffness in the case of calcifications. Boundary conditions included con-straining the vessel such that it was free to move along the Z-axis from one end and restrained from moving in the opposite end via symmetry constraint. This ensured that the coronary vessel structure mimicked a function-al entity within the human body. The loading conditions constituted applying the pressure load to the lumen of the vessel in 16 steps over the range of 0-16 KPa (0-120 mmHg). The static pressure was applied along the lu-minal wall representing the mean physiological blood pressure in the coronary arteries.

Table 1. Material Properties for Arteries, Plaques, Calcifications, and Lipids. [1].

	Young Moduli (E), Pa			Poisson Ratios (P)			Shear Moduli (G), Pa		
	R	**θ**	**z**	**rθ**	**θz**	**zr**	**rθ**	**θz**	**zr**
Artery	10	100	10	0.01	0.27	0.27	50	50	50
Plaque	50	1000	50	0.01	0.27	0.27	50	1000	50
Calcification	10,000	10,000	10,000	0.48	*0.48*	*0.48*			
Lipid	1	1	1	0.48	0.48	0.48			

5 Results and Discussion

The coronary artery obtained for the study was collected from a cadaver with a medical history indicative of severe atherosclerosis. The finite element mesh of vessel lumen was subjected to a maximum diastolic pressure of 16 KPa (120 mmHg) and the resulting stress and strain distributions were examined, Figure 6.

As expected, the model displays corresponding regions of high and low stress throughout the diseased segment. The lipid pool exhibits low stresses because of its flexible and band-like nature which reduces the material's inherent capacity to carry much load. As a consequence of the lipid pool's inability to cope with high stress lev-els, the load applied by the diastolic blood pressure is distributed throughout other materials which collectively attempt to maintain a stable state. Regions of the vessel that exhibited greater stresses were the fibrous plaque, calcium, and segments of the vessel wall. In particular, high stresses are found along the fibrous plaque over-lying the lipid pool. Additionally, calcified regions exhibited higher stress levels compared to their lipid coun-terpart.

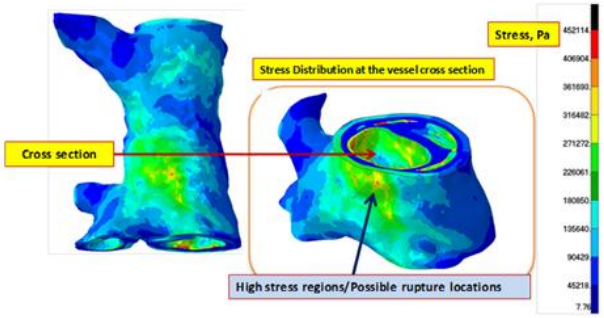

Figure 6. Equivalent stress distributions at a cross section of the vessel.

Despite higher levels of stress and strain, overall plaque stability was not reduced indicating that calcification may play a role in the stabilization of vulnerable plaques. Another critical factor to atherosclerotic plaque stabil-ity is the overall thickness of the vessel wall. Areas with greater thickness also demonstrated lower levels of stress as a result of the distribution of applied pressure over a greater area. The region of highest stress was localized at the plaque shoulder which is the most common location of plaque rupture resulting in thrombotic episodes. This location is most susceptible to plaque rupture because it is the point in the lumen with the sharpest contour resulting in high focal stress concentrations.

Prior studies of human atherosclerotic materials have shown that thin fibrous caps tend to rupture when the static stress or yield strength exceeds 300 KPa [8-11, 15-17]. This value is contingent upon both the thickness of the fibrous cap and the vessel diameter. The current model predicts an equivalent stress of 452 KPa which is 33% higher than the yield stress. The magnitude of the equivalent stress coupled with a cap thickness of ~200 µm indicates a high likelihood of plaque rupture.

Figure 7 illustrates the rupture condition criteria per finite element results. Data for the maximum equivalent and lateral stresses at the cap section along the X (radial) and Y (circumferential) directions were plotted against the rupture strength of human atherosclerotic materials. It is clearly seen from the graph that the lateral stresses in the circumferential direction (through the cap thickness) along with equivalent stresses have ex-ceeded the rupture strength at a static pressure of nearly 11 KPa or 83 mmHg.

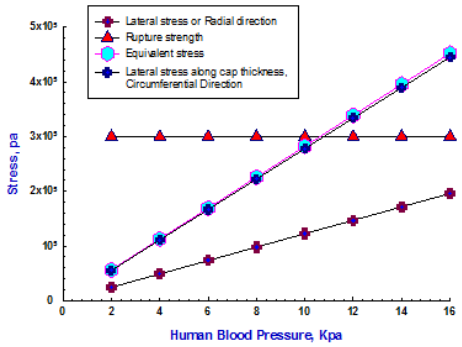

Figure 7. Stress results showing rupture limits and conditions.

Another representation of the stress state in the vessel is shown in Figure 8 which demonstrates a fringe plot of the critical region or the probable rupture site. In either direction whether the stresses are through

the cap thickness or along the radial direction, the critical site remains the same which indicates the presence of a high localized stress area.

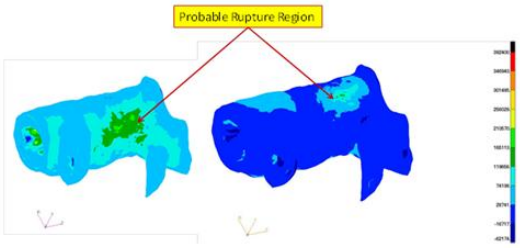

a)Lateral stress along radial direction
b) Cap thru-thickness Stress

Figure 8. Lateral stresses due to blood pressure variations.

Furthermore, the deformed shape of the vessel due to the pressure load is shown in Figure 9. Figure 9(a) represents the deformed shape without an exaggeration or magnification. It is noted that that the section la-beled as a probable rupture region is highlighted in the red color. This supports the data presented in the fringe plots shown in Figure 8 and reaffirm the location of the rupture site.

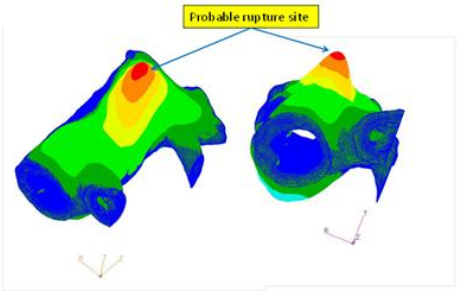

a) Deformed artery b) Magnified of view of the deformed shape

Figure 9. Deformed Artery view of the rupture region.

Figure 9(b) highlights the vessel deformation shape and it shows the indentation at the soft part or the outward bulging region of the normal wall where the calcification site is present. It is further obvious from the figure that the direction of the rupture force is in the through thickness of the cap and it also demonstrates the severity of the rupture as a result of inflated diastolic pressures.

Thus, it can be concluded that in this study we have demonstrated the first use of Cryo-imaging for FEA. The methodology applied has established the “know how” technique to utilize a set of 2D cross-sectional images of sufficiently high resolution to perform advanced analytical modeling of human tissue using the latest available image segmentation algorithms. With these capabilities, several regions of interest that play a role in the overall biomechanical stability of atherosclerosis have been clearly defined. In addition, being able to expand this study into a 3D representation has allowed for the assessment of plaque rupture from several angles in order to pin-point high-risk regions throughout the vessel.

Despite the immense amount of detailed provided by the 3D model and subsequent FEA, there are several limitations that must be kept in mind. For example, the human body is a dynamic environment in which there are several factors that may contribute to overall plaque stability. In addition to biomechanical factors such as blood flow and individual plaque components, there are many molecular mechanisms that constantly remodel the vessel wall. These changes may contribute to strengthening or weakening the plaque. In this study, we were not able to take these molecular factors into account or segment transient components such as elastin or collagen which are thought to also play a role in plaque stability. Furthermore, it must be noted that the hemodynamic conditions inside blood vessels lead to the development of superficial stresses near the vessel walls, which can be divided into two categories; 1) circumferential stress due to pulse pressure variation inside the vessel; 2) shear stress due to blood flow. These conditions were not accounted for in these analyses, only the variation in the diastolic blood pressure was the key element in applying the load to the artery wall.

Lastly, it is crucial for the analyst to ensure that the modeling aspects deliver a true representation of the prob-lem being assessed. For example, extremely fine and/or locally refined meshes near external boundaries may be required in complex structures having many interfaces such as the lipid pool. This can be very computation-ally intensive and calculated data should be checked carefully to ensure that numerical instabilities are not present in the solution. In a simulation having numerical instability, the magnitudes of oscillations are inherently unpredictable resulting in potentially misleading data.

6 Conclusion

This study presents a novel approach for the rendering of advanced 3D models obtained from serial 2D Cryo images and a subsequent finite element analysis. Cryo-imaging carries the intended potential to help establish the groundwork for future ex vivo biomechanical investigations of plaque rupture. It is our hope that further validation of histological components of vulnerable plaques such as collagen, elastin, and possibly even com-ponents of inflammation such as macrophage may be included in future analysis. Moreover, being able to co-register images taken via Cryo to images taken by intravascular imaging modalities such as OCT would allow for in-depth comparison studies of rupture conditions in coronary vessels. Lastly, this research exercise outlays the foundation for future work where the prediction of rupture conditions in a three dimensional perspective is within clinical reach and applicability.

ACKNOWLEDGEMENTS

The authors thank Cuyahoga County Coroner's Office and University Hospitals of Cleveland for supplying specimen. The authors also thank both Mr. Todd Fennimore and Mr. Mark Beno of Case Western Reserve University School of Medicine for their assistance and support.

REFERENCES

[1] Matter CM, Stuber M, Nahrendorf M. Imaging of the unstable plaque: how far have we got? European Heart Journal. 2009; 30: 2566-2574.

[2] Falk E, Shah PK, Fuster V. Coronary plaque disruption. Circulation. 1995;92:657-71

[3] Falk E. Plaque rupture with severe pre-existing stenosis precipitating coronary thrombosis: characteristics of coronary atherosclerotic plaques underlying fatal occlusive thrombi. Br Heart J. 1983;50:127–134.

[4] Virmani R, Kolodgie FD, Burke AP, Farb A, Schwartz SM. Lessons from sudden coronary death: a comprehensive morphological classification scheme for atherosclerotic lesions. Arterioscler Thromb Vasc Biol. 2000;20:1262–1275.

[5] Hansson GK. Inflammation, Atherosclerosis, and Coronary Artery Disease. New England Journal of Medicine. 2005;352:1685-95.

[6] Chau AH et al. Mechanical Analysis of Atherosclerotic Plaques Based on Optical Coherence Tomography. Annals of Biomechanical Engineering 2004; 32:1494-1503.

[7] Ali Abdul-Aziz ; Louis J. Ghosn ; George Y. Baaklini ; Ramakrishna Bhatt; Combined NDE/finite element technique to study the effects of matrix porosity on the behavior of ceramic matrix composites. Proc. SPIE 5046, Nondestructive Evaluation and Health Monitoring of Aerospace Materials and Composites II, 144 (August 4, 2003); doi:10.1117/12.484775.

[8] Davies MJ. A macro and micro view of coronary vascular insult in ischemic heart disease. Circulation. 1990;82(suppl II):II-38 –II-46.

[9] Cheng GC, Loree HM, Kamm R, Fishbein MC, Richard TL. Distribution of Circumferential Stress in Ruptured and Stable Atherosclerotic Lesions. A Structural Analysis With Histopathological Correlation. Circulation 1993;87:1179-1187.

[10] Richardson PD, Davies MJ, Born GV. Influence of plaque configuration and stress distribution on fissuring of coronary atherosclerotic plaques. Lancet 1989;2:941-4

[11] Loree HM, Kamm RD, Stringfellow RG, Lee RT. Effects of fibrous cap thickness on peak circumferential stress in model atherosclerotic vessels. Circulation Research 1992;71:850-8.

[12] Nguyen MS et al. Ex vivo characterization of human atherosclerotic iliac plaque components using cryo-imaging. Journal of Microscopy 2008;232:432–441

[13] ScanIP, Simpleware Ltd, Innovation Centre, University of Exeter, Rennes Drive, EX4 4RN, UK.

[14] Abaqus Finite Element program, SIMULA, Providence, RI 02909 USA.

[15] Imoto et al. Longitudinal Determinants of Plaque Vulnerability. JACC Vol. 46 No. 8, 2005, October 18, 2005:1507-15

[16] Imoto K. et al. Longitudinal Structural Determinants of Atherosclerotic Plaque Vulnerability: A computational Analysis of Stress Distribution Using Vessel Models and Three-Dimensional

Intravascular Ultrasound Imaging. Journal of the American College of Cardiology. 2005;46:1507-1515.

[17] Huang H et al. The Impact of Calcification on the Biomechanical Stability of Atherosclerotic Plaques. Circulation. 2001;103:1051-1056